



OPEN ACCESS

EDITED BY
Darcy E. Wagner,
Lund University, Sweden

REVIEWED BY
Chiharu Ota,
Tohoku University Hospital, Japan
Talya Dayton,
European Molecular Biology Laboratory, Spain

*CORRESPONDENCE
Isabelle Ruchonnet-Metrailler
✉ Isabelle.Ruchonnet-Metrailler@hcuge.ch

RECEIVED 22 March 2023
ACCEPTED 28 July 2023
PUBLISHED 29 August 2023

CITATION
Cardoso dos Santos LM, Avila Y, Schwartz D,
Rougemont A-L, Bochaton-Piallat M-L and
Ruchonnet-Metrailler I (2023) Laser
microdissection, proteomics, and multiplex
immunohistochemistry: a bumpy ride into the
study of paraffin-embedded fetal and pediatric
lung tissues. *Front. Med.* 10:1191205.
doi: 10.3389/fmed.2023.1191205

COPYRIGHT
© 2023 Cardoso dos Santos, Avila, Schwartz,
Rougemont, Bochaton-Piallat and
Ruchonnet-Metrailler. This is an open-access
article distributed under the terms of the
[Creative Commons Attribution License \(CC BY\)](https://creativecommons.org/licenses/by/4.0/).
The use, distribution or reproduction in other
forums is permitted, provided the original
author(s) and the copyright owner(s) are
credited and that the original publication in this
journal is cited, in accordance with accepted
academic practice. No use, distribution or
reproduction is permitted which does not
comply with these terms.

Laser microdissection, proteomics, and multiplex immunohistochemistry: a bumpy ride into the study of paraffin-embedded fetal and pediatric lung tissues

Luis M. Cardoso dos Santos^{1,2}, Yannick Avila^{1,2},
Domitille Schwartz^{3,4}, Anne-Laure Rougemont⁵,
Marie-Luce Bochaton-Piallat¹ and
Isabelle Ruchonnet-Metrailler^{1,2*}

¹Department of Pathology and Immunology, Faculty of Medicine, University of Geneva, Geneva, Switzerland, ²Pediatric Pulmonary Unit, Department of Pediatrics, Gynecology, and Obstetrics, University Hospital of Geneva, Geneva, Switzerland, ³Proteomics Core Facility, Faculty of Medicine, University of Geneva, Geneva, Switzerland, ⁴Bioinformatic Support Platform, Faculty of Medicine, University of Geneva, Geneva, Switzerland, ⁵Department of Pathology, University Hospital of Geneva, Geneva, Switzerland

Background: Knowledge about lung development or lung disease is mainly derived from data extrapolated from mouse models. This has obvious drawbacks in developmental diseases, particularly due to species differences. Our objective is to describe the development of complementary analysis methods that will allow a better understanding of the molecular mechanisms involved in the pathogenesis of rare congenital diseases.

Methods: Paraffin-embedded human pediatric and fetal lung samples were laser microdissected to enrich different lung regions, namely, bronchioli or alveoli. These samples were analyzed by data-independent acquisition-based quantitative proteomics, and the lung structures were subsequently compared. To confirm the proteomic data, we employed an optimized Sequential ImmunoPeroxidase Labeling and Erasing (SIMPLE) staining for specific proteins of interest.

Results: By quantitative proteomics, we identified typical pulmonary proteins from being differentially expressed in different regions. While the receptor for advanced glycation end products (RAGE) and the surfactant protein C (SFTPC) were downregulated, tubulin beta 4B (TUBB4B) was upregulated in bronchioli, compared to alveoli. In fetal tissues, CD31 was downregulated in fetal bronchioli compared to canaliculi. Moreover, we confirmed their presence using SIMPLE staining. Some expected proteins did not show up in the proteomic data, such as SOX-9, which was only detected by means of immunohistochemistry in the SIMPLE analysis.

Conclusion: Our data underline the robustness and applicability of this type of experimental approach, especially for rare paraffin-embedded tissue samples. It also strengthens the importance of these methods for future studies,

particularly when considering developmental lung diseases, such as congenital lung anomalies.

KEYWORDS

human fetal lung tissue, formalin-fixed paraffin embedded (FFPE) lung, human lung development, lung proteome, RAGE expression, SOX-9 expression

1. Introduction

The lung is an essential organ for life in all mammals. Nonetheless, there is still a big gap in the knowledge about its development due to the complexity of the physiology and biological mechanisms occurring in this organ. Consequently, the lack of *in vivo* and *in vitro* models hinders the proper understanding of various pathologies and, in particular, of rare developmental congenital anomalies. To overcome this issue, researchers have been developing new techniques that are able to provide more detailed information using the scarce material that is available from patients, typically formalin-fixed paraffin-embedded (FFPE) tissues. Many biobanks contain a multiplicity of these valuable samples, which can be used to further study these pathologies retrospectively. This type of preservation is particularly attractive due to the convenience of handling the material and its excellent tissue morphology preservation. For protein detection in tissue samples, both in a clinical diagnostic setting and for research issues, immunohistochemistry (IHC) is the gold standard; however, unless multiplexing is used, it does not allow the co-visualization of multiple targets in one section, while tissue availability may become an issue in small biopsy specimens. Immunofluorescence staining came as an alternative but, generally, at the cost of diminished data quality, e.g., autofluorescence (particularly present in lung tissue), photobleaching when acquisitioning big areas of tissue, a limited number of fluorophore combinations, and often the need for different antibodies than those already used in histopathology laboratories.

Herein, we propose a coupled approach to study in-depth the proteome of the human lung, using laser microdissected (LMD) FFPE tissue samples, associated with a multiplexed IHC technique, coined Sequential ImmunoPeroxidase Labeling and Erasing (SIMPLE). The latter will confirm the proteomic data while providing the localization of several target proteins in one tissue section. The LMD technique allows for defining and isolating specific histological structures in the FFPE sections with the enrichment of a defined cellular or tissular compartment, overcoming tissue heterogeneity (1–3). Proteomic studies, particularly LMD-associated proteomics, have been used in the characterization of the human lung. It has been employed to characterize normal lung tissue in FFPE samples, focusing on the extracellular matrix composition (4), or define the lung postnatal developmental protein signature (5). In a pathological context, we previously performed LMD proteomics on congenital pulmonary airway malformation human samples (6). This previous study provided only qualitative data due to a lack of material, a situation that is currently being improved in a follow-up study. The

confirmation of proteomic data using the SIMPLE technique has already been described for different organs (7–9) but, to the best of our knowledge, never in pediatric and fetal lung tissue.

2. Materials and methods

2.1. Tissue sample preparation and laser microdissection

The FFPE blocks of human pulmonary tissue specimens from five fetuses (Ethical Committee 2016-00175) and five healthy lung tissues of postnatal pulmonary lobectomies (Ethical Committee 12-110; [Supplementary Table 1](#)) were cut into 10 μm -thick sections and mounted on Leica PET-membrane slides (76463-320, Leica Microsystems). Postnatal lung tissues were considered “healthy” after microscopic or histological analysis by a pulmonary pathologist. Samples were deparaffinized and hydrated according to standard histological procedures, stained with hematoxylin (S330130-2, Agilent), and stored at 4°C. Laser microdissection was performed in all 10 hematoxylin-stained samples ([Figure 1A](#)), according to the manufacturer’s user guidelines. Briefly, an upright Leica DM6500 microscope, equipped with a CrysLas laser and a Leica CC7000 camera, was used to perform the tissue LMD, where specific tissue fragments were isolated with a UVI 5 $\times/0.12$ microdissection objective, and regions of interest were defined manually with the LAS-AF software (Leica). The isolated fragments were collected in 0.5-ml PCR tubes. We proceeded into an enrichment in the epithelial portions of postnatal and fetal lung tissues from different lung structures: postnatal bronchioli and alveoli, and fetal bronchioli and canaliculi, respectively. It is noteworthy that due to the nature of the technique, the enrichment in the epithelial component was not complete, including as well the immediate surrounding mesenchyme, namely, the bronchiolar muscle layer and capillaries. The structures were selected based on their histological features. Bronchioli, both fetal and postnatal, were defined as well-differentiated airways lined by a pseudo-stratified columnar epithelium or a simple cuboidal epithelium supported by smooth muscle and connective tissue. In the fetal lung at the canalicular stage of development, canaliculi were defined as tubular structures varying from simple to branched, lined by columnar vacuolated epithelium to cuboidal non-vacuolated epithelium. Alveoli were easily recognized, and care was taken not to include medium-sized blood vessels or lymphoid aggregates.

Samples were collected and stored at -20°C . To normalize tissue quantity for subsequent mass spectrometry (MS)-based proteomics, the equivalent of $1.2 \times 10^6 \mu\text{m}^2$ for the bronchioli, fetal

a ratio of $1.2 \times 10^6 \mu\text{m}^2$ per 100 μL . They were sonicated (6×30 s) at 70% amplitude and 0.5 pulses and kept on ice for 30 s between each cycle of sonication. To remove residual paraffin and sufficiently reverse formaldehyde crosslinks, samples were heated for 1 h at 95°C , then 1 h at 65°C , followed by a second round of sonication. For 100 μL of the sample, 2 μL of 50 mM dithioerythritol was then added, and the reduction was carried out at 37°C for 1 h. Alkylation was performed by adding 2 μL of 400 mM iodoacetamide (per 100 μL of sample) for 1 h at room temperature in the dark. Overnight digestion was performed at 37°C with 2 μL of freshly prepared trypsin at 0.1 $\mu\text{g}/\mu\text{L}$ (V5111, Promega) in 50 mM ammonium bicarbonate (per 100 μL of sample). To remove RapiGest, samples were acidified with 5 μL of 10% trifluoroacetic acid (91719, Sigma-Aldrich), heated at 37°C for 45 min, and centrifuged for 10 min at $17,000 \times g$. Each sample was desalted with a C18 microspin column (Harvard Apparatus) according to the manufacturer's instructions, completely dried under a speed vacuum, and stored at -20°C .

2.3. Liquid chromatography–electrospray ionization tandem mass spectrometry

Samples were resuspended in 12 μL of loading buffer (5% CH_3CN , 0.1% CH_2O_2). iRT peptides (Biognosys AG, Switzerland) were added to each sample, and 4 μL of peptides were injected into the column. Liquid chromatography–electrospray ionization tandem mass spectrometry (LC/ESI-MS/MS) was performed on an Orbitrap Fusion Lumos Tribrid mass spectrometer (Thermo Fisher Scientific, USA) equipped with an Easy nLC1200 liquid chromatography system (Thermo Fisher Scientific, USA). Peptides were trapped on an Acclaim pepmap100, C18, 3 μm , 75 $\mu\text{m} \times 20$ mm nano trap-column (Thermo Fisher Scientific, USA) and separated on a 75 $\mu\text{m} \times 500$ mm, C18 ReproSil-Pur (Dr. Maisch GmbH, Germany), 1.9 μm , 100 \AA , homemade column. The analytical separation was run for 135 min using a gradient of $\text{H}_2\text{O}/\text{CH}_2\text{O}_2$ (99.9%/0.1%—solvent A) and $\text{CH}_3\text{CN}/\text{H}_2\text{O}/\text{CH}_2\text{O}_2$ (80.0%/19.9%/0.1%—solvent B). The elution gradient was run from 8 to 28% of solvent B in 110 min, to 42% of solvent B in 25 min, then to 95% solvent B in 5 min, with a final stabilization step of 20 min in 95% solvent B. The flow rate was 250 nl/min, with a total run time of 160 min. Data-Independent Acquisition (DIA) was performed with a precursor full scan (MS1) at a resolution of 60,000 full widths at half maximum (FWHM), followed by 30 product ion scans (MS2) with fixed wide precursor isolation windows. MS1 was performed in the Orbitrap with an AGC target of 1×10^6 , a maximum injection time of 50 ms, and a scan range from 400 to 1,240 m/z . DIA MS2 was performed in the Orbitrap using higher-energy collisional dissociation (HCD) at 30%. Isolation windows were set to 28 m/z with an AGC target of 1×10^6 and a maximum injection time of 54 ms. Due to the typically low yield of protein, we performed a single run of LC-MS/MS in five different biological samples for each structure type.

2.4. Proteomic data analysis

The DIA raw files were loaded into Spectronaut v.15 (Biognosys) and analyzed by directDIA using default settings.

Briefly, data were searched against the Human Protein Reference Database (Uniprot; 20660 entries). Trypsin was selected as the enzyme, with one potential missed cleavage. Variable amino acid modifications were oxidized methionine and deaminated (NQ). The fixed amino acid modification was carbamidomethyl cysteine. Both peptide precursor and protein false discovery rate (FDR) were controlled at 1% ($Q\text{-value} < 0.01$). Single-hit proteins were excluded. For quantitation, the top 3 precursor area per peptide was used, “only protein group-specific” was selected as the proteotypicity filter, and normalization was set to “global normalization.” The quantitative analysis was performed with the MapDIA tool, using the precursor quantities extracted from Spectronaut output. No further normalization was applied. The following parameters were used: min peptides = 2, max peptides = 10, min correl = -1 , Min_DE = 0.01, max_DE = 0.99, and experimental_design = independent design. For subsequent analysis, each group (postnatal and fetal bronchioli, alveoli, and canaliculi) was composed of five different biological samples. Proteins were considered to have significantly changed in abundance with an FDR of ≤ 0.05 and an absolute fold change $\text{FC} \geq |1.5|$ ($\log_2\text{FC} \geq |0.58|$). Gene Ontologies term enrichment analysis, as well as associated plots, were performed with ClusterProfiler (10, 11) R package, using the EnrichGO function. Enrichment tests were calculated for GOterms, based on the hypergeometric distribution. The enrichment p -value cutoff was set to 0.05, and the Q -value cutoff to 0.01. The gofilter function was used prior to the cnetplot drawing to filter results at specific levels. To determine protein cellular localization, we used the NeXtProt knowledge database (reviewed and annotated for the human proteome) and extracted the gold and silver annotated proteins for four Gene Ontologies and Uniprot Subcellular Location (SL) terms: plasma membrane (GO:0005886 and SL-0036), extracellular matrix (GO:0031012), cytosol (GO:0005829 and SL-0091), and nuclear (GO:0005634 and SL-0191; Supplementary Table 2). The mass spectrometry proteomics data (DIA raw files) have been deposited to the ProteomeXchange Consortium via the PRIDE (12) partner repository with the dataset identifier PXD040654.

2.5. Sequential Immunoperoxidase Labeling and Erasing

A schematic representation of the SIMPLE staining is shown in Figure 1B. Three micrometer FFPE tissue sections were mounted on TruBond™ 380 slides (50-364-505, Electron Microscopy Sciences), placed at 54°C overnight before going through deparaffination, 4 \times 10 min in Ultraclear (3905.9010PE, Avantor), and hydrated in a series of graded alcohols (95%–50%) to distilled water. The specimen went through heat-induced epitope retrieval (HIER) in either citrate pH 6.0 or tris-EDTA pH 9.0 buffers, according to antibody specification, using a Bio SB TintoRetriever Pressure Cooker (BSB-7087, Bio SB), set at low pressure for 10 min. After HIER, slides were cooled down in an ice bath for 15 min, and endogenous peroxidases were quenched with DAKO REAL Peroxidase-Blocking Solution (S202386-2, Agilent) for 5 min. In addition to blocking unspecific antibody binding using Serum-Free

Protein Block (X0909, Agilent) for 10 min, an Avidin/Biotin Blocking Kit (ab64212, Abcam) was used for 10 min to block endogenous avidin and biotin binding sites, respectively. Primary antibodies (Supplementary Table 3) were then incubated for 1 h at room temperature.

The following antibodies were used: anti-CD31 (66065-2-Ig, Proteintech), anti-surfactant protein C (SFTPC, AB3786, Merck), homemade anti- α -smooth muscle actin [clone 1A4, α -SMA, or ACTA2 (13)], anti-receptor for advanced glycation end products (RAGE, ab3611, Abcam), anti-tubulin beta 4B (TUBB4B, sc-134230, Santa Cruz), and anti-SOX-9 (AB5535, Millipore). As negative controls, mouse IgG1 (BE0083, Biorcell) or IgG2a (MAB0031, R&D Systems) isotype control and rabbit IgG isotype control (10500C, Invitrogen) were used. Goat anti-mouse IgG (1:250, 115-066-146, Jackson ImmunoResearch) and goat anti-rabbit IgG (1:250, 111-066-144, Jackson ImmunoResearch) secondary biotinylated antibodies were incubated for 30 min at room temperature, followed by another 30 min room temperature incubation with streptavidin or horseradish peroxidase (1:300, P0397, Agilent). Staining was obtained by using an alcohol-soluble peroxidase substrate and 3-amino-9-ethylcarbazole (AEC, AC1331003, DCS Innovative Diagnostik-Systeme). Slides were counterstained with hematoxylin and finally coverslipped with Aquatex mounting solution (1.08562.0050, Merck) or PBS before whole-slide image scanning at 20 \times magnification using a Zeiss AxioScan.Z1.

After image acquisition, slides were de-coverslipped by immersion in dH₂O. AEC staining was then removed by sequential washing in 50% (1 min)/75% (3 min)/95% (8 min, shaking every 2 min)/75% (2 min)/50% (1 min) ethanol solutions, followed by rehydration in dH₂O. Antigen and antibody complex stripping was achieved via HIER (10 min at high pressure). Mouse (1:25, 115-007-003; Jackson ImmunoResearch) and rabbit (1:25, 111-007-003, Jackson ImmunoResearch) fragment antigen-binding solutions targeted against primary antibodies host species were used to prevent undesired binding between not fully stripped antigen-antibody complex from the previous stain and the secondary biotinylated antibodies of the subsequent staining. At this point, slides re-entered the same process of staining as described above, starting with the Serum-Free Protein Block. All antibodies and Streptavidin/HRP were diluted in DAKO Antibody Diluent (S0809, Agilent).

2.6. SIMPLE data processing

Whole-slide multiplexed images originating from the same tissue section and consisting of five antigen revelation were processed with a custom-made framework developed in Matlab R2022b (The MathWorks). Briefly, these large data (tens of gigabytes) were aligned at a cellular level according to the same reference image using manual control points pairing to infer affine transformations. Afterward, hematoxylin and AEC chromogenic stainings of each image were unmixed using an adaptation of the study of Landini and colleagues (14) optimized for computation speed and processing of large datasets. Finally, a single multiplexed image, with one channel per antigen and the related metadata,

was exported in the OME-TIFF file format. These newly generated images could then be opened and processed with QuPath0.3.2 (15).

3. Results

3.1. Laser microdissection and proteomic analysis

For proteomic purposes, we collected five samples from either postnatal or fetal lung tissue (Supplementary Table 1) that were laser microdissected, enriching the epithelial portions of bronchioli, fetal bronchioli, alveoli, and canaliculi structures (Figures 2A, B). Noteworthy is the fact that, due to the structure of alveoli and canaliculi, these compartments corresponded not only to the alveoli and canaliculi but also to the immediate surrounding mesenchyme. For each individual, several tissue fragments were microdissected (as shown in Figures 2A, B), where the minimum amount of selected area (SA) tissue was calculated to include the laser-destroyed area (LA) and provide enough material to allow downstream proteomic analysis. Principal component analysis (PCA) confirmed that LMD was technically reproducible and, most importantly, that samples from the same experimental group were, in general, close in their protein profile, thus strengthening the proteomics analysis (Supplementary Figure 1). The main differences in protein pattern were found in PC1 between alveoli and fetal bronchioli (43% of the model variability). Moreover, we observed that the alveolar samples were the only group that presented considerable variability. Additionally, one of the samples from the postnatal bronchioli was clearly apart from the rest of the samples in the group (Supplementary Figure 1, sample E5), which we decided to maintain for discussion purposes.

We focused on the proteomic differences between bronchioli and alveoli (Figure 2C) or their fetal counterparts—fetal bronchioli and canaliculi (Figure 2D). For the two comparisons, we detected a total of 2,509 and 2,548 proteins, respectively, which were then assigned a cellular localization. The proportion of the assigned localizations was similar in the two sets of data, roughly corresponding to 60% nuclear, 47% cytoplasmic, 30% plasma membrane, or 6% extracellular matrix (Supplementary Figure 2, Supplementary Table 2). Of note, in both comparisons, 44% of all proteins shared at least two cellular localizations.

For the purpose of this study, among the 592 and 484 proteins that were found differentially expressed [FDR < 0.05; fold change (\log_2) \geq 0.58] in the comparison of bronchioli vs. alveoli and fetal bronchioli vs. canaliculi, respectively, we focused on proteins that were characteristic of bronchial and alveolar structures. For the bronchial compartment, we selected TUBB4B and ACTA2, markers of ciliary epithelium and airway smooth muscle cells, respectively. For the alveolar structures, we selected the RAGE, SFTPC, and CD31 as markers of alveolar type I cells, alveolar type II cells, and endothelial cells, respectively. In postnatal tissue, TUBB4B and ACTA2 were upregulated in bronchioli, compared to alveoli. As expected, we found RAGE, SFTPC, and CD31 significantly downregulated in bronchioli, compared to alveoli (Figure 2Ca). Regarding the fetal tissues (canalicular developmental stage),

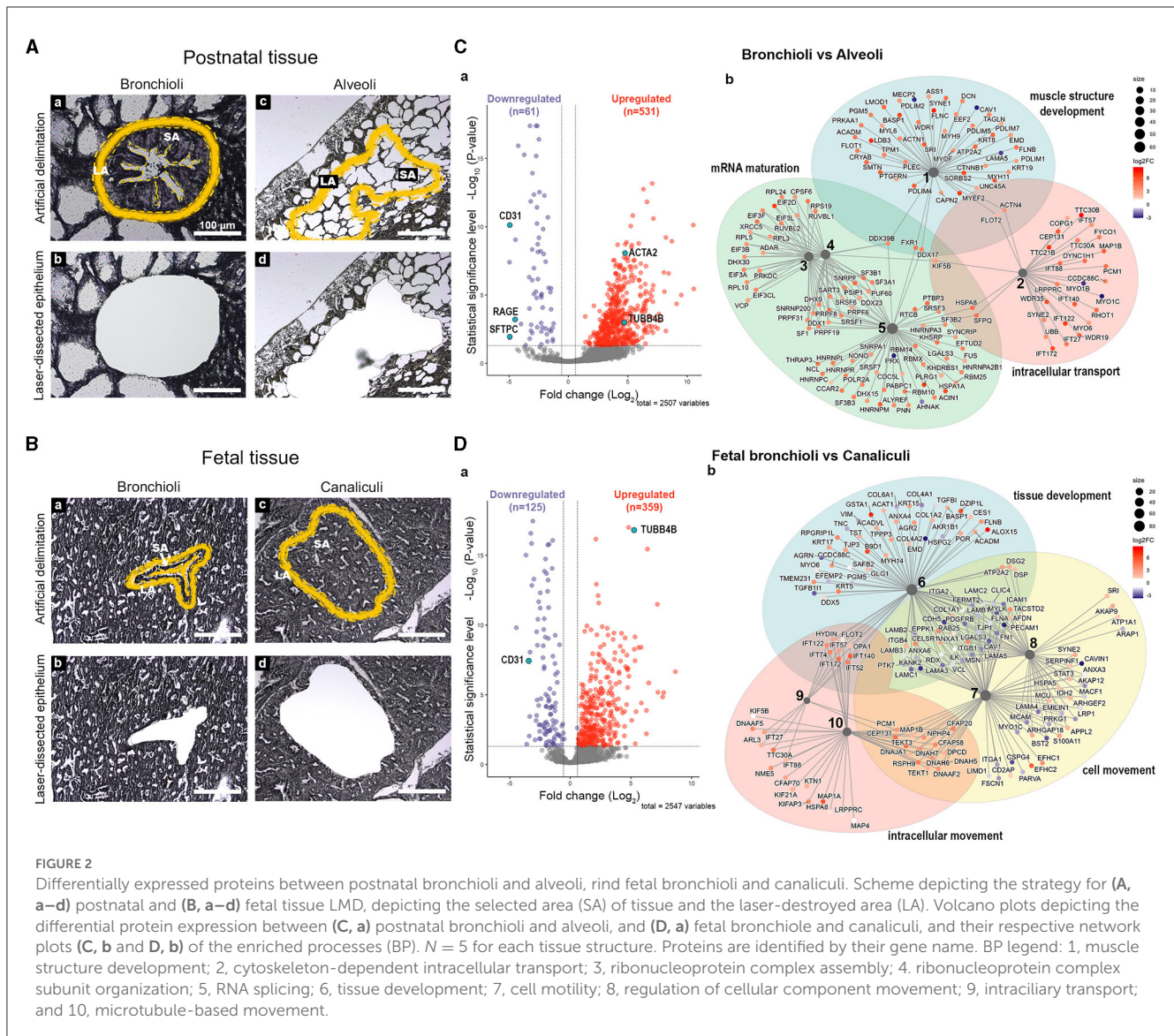


FIGURE 2
 Differentially expressed proteins between postnatal bronchioli and alveoli, and fetal bronchioli and canaliculi. Scheme depicting the strategy for (A, a–d) postnatal and (B, a–d) fetal tissue LMD, depicting the selected area (SA) of tissue and the laser-destroyed area (LA). Volcano plots depicting the differential protein expression between (C, a) postnatal bronchioli and alveoli, and (D, a) fetal bronchiole and canaliculi, and their respective network plots (C, b and D, b) of the enriched processes (BP). $N = 5$ for each tissue structure. Proteins are identified by their gene name. BP legend: 1, muscle structure development; 2, cytoskeleton-dependent intracellular transport; 3, ribonucleoprotein complex assembly; 4, ribonucleoprotein complex subunit organization; 5, RNA splicing; 6, tissue development; 7, cell motility; 8, regulation of cellular component movement; 9, intracellular transport; and 10, microtubule-based movement.

RAGE and SFTPC were considered not present or below the threshold of detection, not allowing the subsequent processing and quantification. Moreover, while TUBB4B expression was increased in fetal bronchioli, CD31 expression was increased in canaliculi (Figure 2Da).

Following the differential protein expression analysis, we performed the Gene Ontology enrichment of biological processes (BP) for postnatal and fetal samples (Supplementary Table 4). For visualization purposes, the graphic representations of the enriched BP of the comparison “bronchioli vs. alveoli” (Figure 2Cb) and “fetal bronchioli vs. canaliculi” (Figure 2Db) did not include all branches of the GO tree. Five selected GO terms enriched in bronchiole compared to alveoli were grouped into three main classes related to muscle structure development, intracellular transport, and mRNA maturation (Figure 2Cb). Similarly, in the fetal tissue, BP enriched in fetal bronchioli compared to canaliculi was grouped into three main classes related to tissue development, intracellular movement, and cell movement (Figure 2Db).

3.2. SIMPLE staining

To confirm the proteomic data, we performed SIMPLE staining, a technique developed by Glass and colleagues (7). Following the SIMPLE scheme depicted in Figure 1, fetal and postnatal lung samples ($n = 6$ and $n = 9$, respectively, with staining performed in triplicate for some of them) were stained for the different markers previously mentioned (Figure 3). For a proper validation of the technique, in addition to the tissue samples used for proteomic analysis, new samples were introduced (Supplementary Table 1). The following order of primary antibodies were used: first round staining CD31 and SFTPC, second round staining RAGE and ACTA2, and third round staining TUBB4B. For coverslip fixation, we chose PBS since the use of Aquatex mounting solution was shown to affect, when using a primary antibody cocktail, the second antibody revelation. Aquatex was only used in the second revelation if a heat-induced antibody stripping was planned or if digital acquisition was not immediately possible. As

expected and corroborating the proteomic data, RAGE, SFTPC, and CD31 were detected in alveolar areas of postnatal tissue (Figure 3A, panel a), while they were virtually absent in fetal canaliculi (Figure 3B, panel d). Moreover, RAGE and SFTPC were restricted to postnatal alveoli and not present in other lung structures, while CD31 was evidently expressed by vascular endothelial cells of both postnatal (Figure 3A, panel c) and fetal tissues (Figure 3B, panel f). Regarding the bronchial regions, TUBB4B staining was detected in ciliary epithelial cells of both postnatal (Figure 3A, panel b) and fetal tissues (Figure 3B, panel e), with ACTA2 staining being specific for the airway smooth muscle layer surrounding the bronchioli. Alongside CD31, ACTA2 expression was expectedly present in vessels, staining vascular smooth muscle cells (Figures 3A, panel c, B, panel f).

SOX-9, a well-known marker of chondrocyte differentiation, has been shown to play a central role in lung branching morphogenesis (16). Unexpectedly, SOX-9 was absent from the fetal data, which could be related either to a low abundance of this protein, illustrating a limitation of this proteomic pipeline, or to the age of the fetal samples. Indeed, these samples were of 19 and 21 gestational weeks (GW), and when performing IHC staining, SOX-9 was found at either low levels of expression or was absent (Supplementary Figure 3). To better characterize SOX-9 expression, we performed IHC staining, where SOX-9 was indeed detected at several early gestational time points (Figure 4), corroborating the results from others (16). In particular, we observed a strong expression of SOX-9 from our earliest time point, 12 gestational weeks (GW), until approximately 21 GW, where its expression decreased significantly (Figure 4). It is noteworthy that, at 14 and 16 GW, SOX-9 was found to be highly expressed (data not shown). At later time points (26GW and postnatally), SOX-9 expression was, as expected, only detectable in cartilage tissue. Notably, in the course of our SIMPLE staining, we observed that, whenever SOX-9 was expressed, we were not able to detect RAGE expression. RAGE expression was only observed at later developmental stages when SOX-9 expression was either low or absent (19–21 GW), gradually increasing until birth (26 GW postnatal; Figure 4). To the best of our knowledge, this is the first description showing a timeline of RAGE protein expression in human fetal lungs.

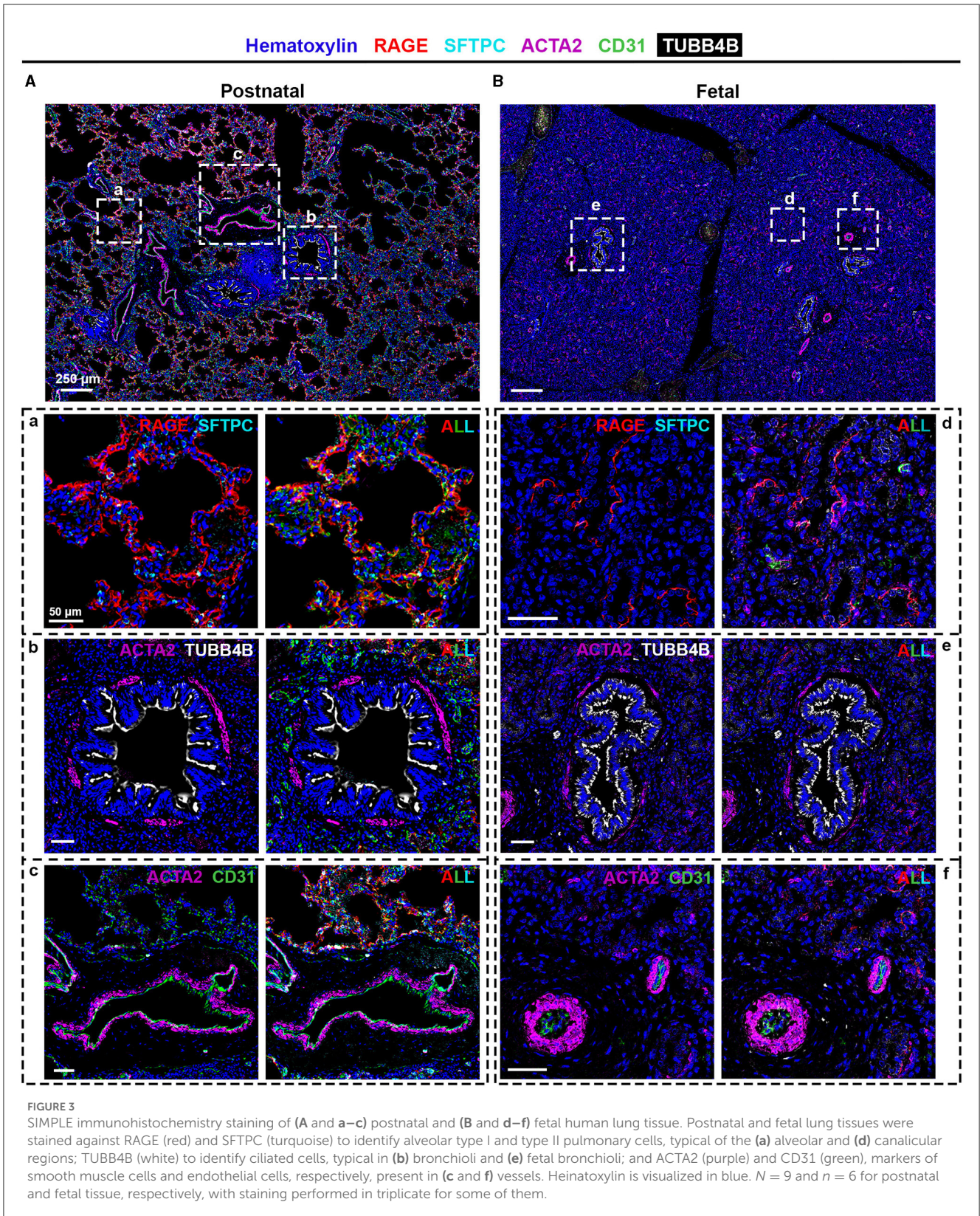
4. Discussion

Human lung samples, especially to study rare developmental diseases, are difficult to obtain. In addition to the limited number of cases, collecting good-quality retrospective samples of lung malformation or fetal lung cases is a real challenge. Fetal samples are also known to present preservation issues due to the nature of the events that originate the collection of these tissues. In this report, we have shown that, although the preservation process might not have been ideal, sample preparation and enrichment succeeded in creating samples of satisfying quality and reproducibility, which allowed the subsequent comparative proteomic analysis. Nonetheless, we have decided to maintain samples of lower quality, such as sample E5 (Supplementary Figure 1), to exemplify some of the caveats of this technique, which requires extensive handling in the

preparation of the protein samples. In particular, sample E5 presents a high degree of missing values (represented in black in Supplementary Figure 1B), and this may have several origins, such as technical issues in LMD or sample preparation or tissue preservation. Interestingly, this sample shares the same source of tissue as sample G3 (alveoli), which also presents a high degree of missing values. However, the alveolar samples (G1–G5) presented the highest degree of variation intra-group, most probably due to the high number of missing values. In addition to the abovementioned possible causes, differences in the honeycomb-like structure of alveoli might also affect the expected amount of obtained protein.

Even though we took into consideration the suggested LMD areas, tissues may vary in structure, i.e., different proportions of cells to air space. Following the data quality validation, we corroborated our proteomic data by performing the SIMPLE technique, where we detected markers of bronchial and alveolar structures in healthy postnatal tissue and, when expected, in fetal tissue. This technique has been widely employed in mouse and human tissues (7, 8), with most of these studies using tumor samples. In the study by Tsujikawa and colleagues, the authors performed an 11-round heat-mediated antibody stripping, which is mainly achievable due to the nature of the tissue. One of the main disadvantages of working with lung samples is their fragility, related to their honeycomb-like structure, in contrast to previous studies in the literature reporting results of the technique in more solid lung tumor samples. In this study, we have empirically experienced that, upon five rounds of HIERS, tissue degradation is quite extensive, which will certainly affect the specificity and reproducibility of the immunostaining. Other factors should be taken into consideration for optimal immunostaining, such as (i) primary antibody specificity for species/tissues and cross-reaction of the secondary antibodies when using primary antibody cocktails; (ii) antibody order, since not all epitopes present the same resistance to the chemical, mechanical, and thermal manipulations during the staining process; and (iii) balance between antibody stripping strength and tissue integrity by testing the required conditions for a smooth, while proper, antibody removal.

We have also raised awareness of the limitations of a proteomic approach. As a proof of concept, we demonstrated that the transcription factor SOX-9, an important factor for cell differentiation, was not detected by proteomics but was identified by IHC as being expressed early in development. The study by Danopoulos and colleagues corroborated our data, showing SOX-9 expression in fetal lung tissue during the pseudoglandular stage (4–16 weeks) until the canalicular stage (16–20 weeks) when SOX-9 expression starts decreasing (16). By performing IHC staining at different gestational time points, we observed that, in our samples, SOX-9 expression is lost between 19 and 21 GW. The variability might be related to the incertitude of the time of fecundation and its annotation or simply due to intrinsic biological variability. Therefore, the lack of SOX-9 signal in our proteomic data was most probably due to either a below-the-threshold level or absence of expression. In addition to a low basal level of protein expression that would not allow its proper detection, other possibilities could be related to the expected low amount of extracted protein from FPFE tissue or to the fact that nuclear proteins usually are not



as easily extracted or detected as cytoplasmic ones. Importantly, together with the SOX-9 timeline, we have demonstrated, to the best of our knowledge, for the first time, the timeline protein expression of RAGE. Its expression is inversely correlated with

SOX-9 expression. Interestingly, our study complements one by Clair and colleagues where they characterized RAGE expression, by LC-MS-based proteomic and Western blot, at 10 postnatal time points, from postnatal day 1 to 8 years (5). Finally, this study

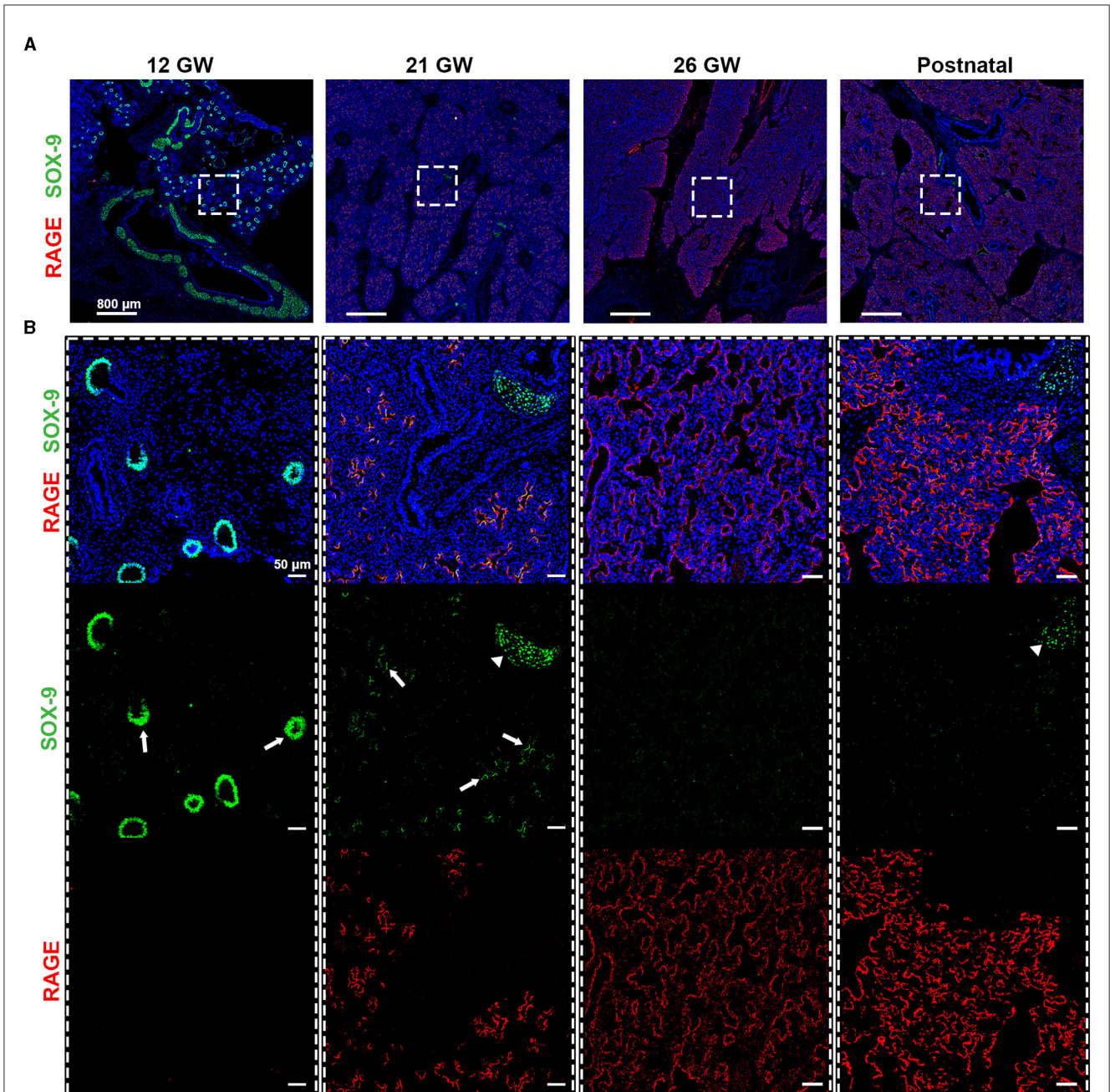


FIGURE 4

(A) Timeline for RAGE (red) and SOX-9 (green) expression in fetal tissues of 12, 21, and 26 gestational weeks (GW) and in postnatal tissue (10 days). (B) Magnification of the region of interest from the upper panel, where we can observe in separate, SOX-9 and RAGE. SOX-9 is expressed at earlier timepoints in canaliculi (arrows) and this expression is lost with the differentiation of airway cells. The loss of SOX9 is concomitant with the beginning of RAGE expression in early alveolar type I cells (in red). SOX-9 can also be found in the cartilage tissue (arrow heads). Hematoxylin is visualized in blue. $N = 3$ for each timepoint of the fetal tissue. Staining was performed in replicate for some tissue.

came as a technical proof of concept for LMD-based proteomic analysis completed using SIMPLE multiplex staining, which will allow us to apply this approach in other contexts, such as in lung developmental diseases (e.g., congenital pulmonary airways malformations) where tissue accessibility and preservation are not optimal and alternatives not available.

Overall, and notwithstanding the intrinsic technical limitations of our pipeline, the results confirm the applicability and

reproducibility of proteome-based analysis in FFPE pediatric lung tissues. We showed, by hand-picking specific markers, the differences between distinct lung structures (bronchioli, alveoli, and vessels) and developmental states (fetal and postnatal tissue). Moreover, we have shown that proteomic data should be confirmed by other approaches, such as classical immunostaining, especially in the case of proteins of difficult extraction or low abundance.

Data availability statement

The original contributions presented in the study are publicly available. This data can be found in the repository PRIDE: dataset identifier PXD040654, <https://www.ebi.ac.uk/pride/archive/projects/PXD040654>.

Ethics statement

The studies involving human participants were reviewed and approved by Ethical Committee 2016-00175, Ethical Committee 12-110. Written informed consent to participate in this study was provided by the participants' legal guardian/next of kin.

Author contributions

LC, YA, and IR-M contributed to conception and design of the study and the writing of the manuscript. LC and YA performed the practical work. DS contributed to the analysis of the proteomic data and the generation of proteomic-related figures and tables. A-LR provided the human specimens. M-LB-P contributed to the design of the study and provided reagents. All authors contributed to manuscript revision, read, and approved the submitted version.

Funding

This work was supported by the Ligue Pulmonaire Genevoise, the Fondation Privée de HUG (#RS07-06), and the Fondation Prim'Enfance. Open access funding by University of Geneva.

References

- Jancelewicz T, Nobuhara K, Hawgood S. Laser microdissection allows detection of abnormal gene expression in cystic adenomatoid malformation of the lung. *J Pediatr Surg.* (2008) 43:1044–51. doi: 10.1016/j.jpedsurg.2008.02.027
- Lezmi G, Verkarre V, Khen-Dunlop N, Vibhushan S, Hadchouel A, Rambaud C, et al. FGF10 Signaling differences between type I pleuropulmonary blastoma and congenital cystic adenomatoid malformation. *Orphanet J Rare Dis.* (2013) 8:130. doi: 10.1186/1750-1172-8-130
- Drummond E, Nayak S, Pires G, Ueberheide B, Wisniewski T. Isolation of amyloid plaques and neurofibrillary tangles from archived Alzheimer's disease tissue using laser-capture microdissection for downstream proteomics. *Methods Mol Biol.* (2018) 1723:319–34. doi: 10.1007/978-1-4939-7558-7_18
- Herrera JA, Mallikarjun V, Rosini S, Montero MA, Lawless C, Warwood S, et al. Laser capture microdissection coupled mass spectrometry (LCM-MS) for spatially resolved analysis of formalin-fixed and stained human lung tissues. *Clin Proteomics.* (2020) 17:24. doi: 10.1186/s12014-020-09287-6
- Clair G, Bramer LM, Misra R, McGraw MD, Bhattacharya S, Kitzmiller JA, et al. Proteomic analysis of human lung development. *Am J Respir Crit Care Med.* (2021) 205:208–18. doi: 10.1164/rccm.202008-3303OC
- Barazzone-Argiroffo C, Lascano Maillard J, Vidal I, Bochaton-Piallat ML, Blaskovic S, Donati Y, et al. New insights on congenital pulmonary airways malformations revealed by proteomic analyses. *Orphanet J Rare Dis.* (2019) 14:272. doi: 10.1186/s13023-019-1192-4
- Glass G, Papin JA, Mandell JW. SIMPLE: a sequential immunoperoxidase labeling and erasing method. *J Histochem Cytochem.* (2009) 57:899–905. doi: 10.1369/jhc.2009.953612
- Tsujikawa T, Kumar S, Borkar RN, Azimi V, Thibault G, Chang YH, et al. Quantitative multiplex immunohistochemistry reveals myeloid-inflamed tumor-immune complexity associated with poor prognosis. *Cell Rep.* (2017) 19:203–17. doi: 10.1016/j.celrep.2017.03.037
- Akturk G, Sweeney R, Remark R, Merad M, Gnjatic S. Multiplexed immunohistochemical consecutive staining on single slide (MICSSS): multiplexed chromogenic IHC assay for high-dimensional tissue analysis. *Methods Mol Biol.* (2020) 2055:497–519. doi: 10.1007/978-1-4939-9773-2_23
- Yu G, Wang LG, Han Y, He QY. clusterProfiler: an R package for comparing biological themes among gene clusters. *OmicS.* (2012) 16:284–7. doi: 10.1089/omi.2011.0118
- Wu T, Hu E, Xu S, Chen M, Guo P, Dai Z, et al. clusterProfiler 4.0: a universal enrichment tool for interpreting omics data. *Innovation.* (2021) 2:100141. doi: 10.1016/j.xinn.2021.100141
- Perez-Riverol Y, Bai J, Bandla C, Garcia-Seisdedos D, Hewapathirana S, Kamatchinathan S, et al. The PRIDE database resources in 2022: a hub for mass spectrometry-based proteomics evidences. *Nucleic Acids Res.* (2021) 50:D543–52. doi: 10.1093/nar/gkab1038

Acknowledgments

We thank the Proteomics and Bioimaging core facilities of the CMU, University of Geneva, for their equipment, advice, and help. In particular, we thank Nicolas Liaudet from the Bioimaging core facility for his help in the development of the proper software for image processing and Dre Labidi-Galy, from the Department of Medicine of the Hôpitaux Universitaires de Genève, for providing the necessary technical support related to the SIMPLE protocol. We also thank Dr. Andrew Vidal for providing some of the human specimens used in this study.

Conflict of interest

The authors declare that the research was conducted in the absence of any commercial or financial relationships that could be construed as a potential conflict of interest.

Publisher's note

All claims expressed in this article are solely those of the authors and do not necessarily represent those of their affiliated organizations, or those of the publisher, the editors and the reviewers. Any product that may be evaluated in this article, or claim that may be made by its manufacturer, is not guaranteed or endorsed by the publisher.

Supplementary material

The Supplementary Material for this article can be found online at: <https://www.frontiersin.org/articles/10.3389/fmed.2023.1191205/full#supplementary-material>

13. Skalli O, Ropraz P, Trzeciak A, Benzonana G, Gillessen D, Gabbiani G. A monoclonal antibody against alpha-smooth muscle actin: a new probe for smooth muscle differentiation. *J Cell Biol.* (1986) 103:2787–96. doi: 10.1083/jcb.103.6.2787
14. Landini G, Martinelli G, Piccinini F. Colour deconvolution: stain unmixing in histological imaging. *Bioinformatics.* (2020) 37:1485–7. doi: 10.1093/bioinformatics/btaa847
15. Bankhead P, Loughrey MB, Fernández JA, Dombrowski Y, McArt DG, Dunne PD, et al. QuPath: open source software for digital pathology image analysis. *Sci Rep.* (2017) 7:16878. doi: 10.1038/s41598-017-17204-5
16. Danopoulos S, Alonso I, Thornton ME, Grubbs BH, Bellusci S, Warburton D, et al. Human lung branching morphogenesis is orchestrated by the spatiotemporal distribution of ACTA2, SOX2, and SOX9. *Am J Physiol Lung Cell Mol Physiol.* (2018) 314:L144–9. doi: 10.1152/ajplung.00379.2017